bioRxiv preprint doi: https://doi.org/10.1101/2023.02.28.530224; this version posted March 1, 2023. The copyright holder for this preprint (which was not certified by peer review) is the author/funder, who has granted bioRxiv a license to display the preprint in perpetuity. It is made available under aCC-BY 4.0 International license.

1 **Lipofuscin-like autofluorescence within microglia and its impact on studying microglial**
2 **engulfment**

3 **Jacob M. Stillman[1,2#], Francisco M. Lopes[1#], Jing-Ping Lin[3], Kevin Hu[3], Daniel S. Reich[3],**
4 **Dorothy P. Schafer[1*]**
5
6 **[#]Authors contributed equally**
7 ***Corresponding Author:** dorothy.schafer@umassmed.edu
8
9
10 [1] Department of Neurobiology, Brudnick Neuropsychiatric Research Institute, University of
11 Massachusetts Chan Medical School, Worcester, MA 01605, USA
12
13 [2] Department of Neurobiology, Brudnik Neuropsychiatric Research Institute, University of Massachusetts
14 Chan Medical School, Worcester, MA, USA; University of Massachusetts Chan Morningside Graduate
15 School of Biomedical Sciences, Neuroscience Program, Worcester, MA, USA.
16
17 [3] Translational Neuroradiology Section, National Institute of Neurological Disorders and Stroke, National
18 Institutes of Health, Bethesda, MD 20892, USA

bioRxiv preprint doi: https://doi.org/10.1101/2023.02.28.530224; this version posted March 1, 2023. The copyright holder for this preprint (which was not certified by peer review) is the author/funder, who has granted bioRxiv a license to display the preprint in perpetuity. It is made available under aCC-BY 4.0 International license.

19 **Abstract**

20 Engulfment of cellular material and proteins is a key function for microglia, a resident
21 macrophage of the central nervous system (CNS). Among the techniques used to measure
22 microglial engulfment, confocal light microscopy has been used the most extensively. Here, we
23 show that autofluorescence (AF), likely due to lipofuscin and typically associated with aging, can
24 also be detected within microglial lysosomes in the young mouse brain by light microscopy. This
25 lipofuscin-AF signal accumulates first within microglia and increases with age, but it is not
26 exacerbated by amyloid beta-related neurodegeneration. We further show that this lipofuscin-AF
27 signal within microglia can confound the interpretation of antibody-labeled synaptic material within
28 microglia in young adult mice. Finally, we implement a robust strategy to quench AF in mouse,
29 marmoset, and human brain tissue.

30

bioRxiv preprint doi: https://doi.org/10.1101/2023.02.28.530224; this version posted March 1, 2023. The copyright holder for this preprint (which was not certified by peer review) is the author/funder, who has granted bioRxiv a license to display the preprint in perpetuity. It is made available under aCC-BY 4.0 International license.

31 **Introduction**

32 Microglia are highly phagocytic tissue-resident macrophages of the central nervous
33 system (CNS). While the phagocytic activity of microglia has historically been attributed to clearing
34 dead or dying cells, the list of microglial phagocytic substrates has expanded in recent years to
35 include synaptic material[1-4], extracellular matrix proteins[5], and protein aggregates (amyloid beta,
36 tau, etc.)[6]. From this work, the engulfment of cellular and protein material by microglia has been
37 shown to regulate synaptic connectivity and modulate neurodegenerative phenotypes[1-4].
38 Microglial engulfment is also an emerging target for therapeutic intervention in diseases ranging
39 from Alzheimer's disease to schizophrenia[7-9]. Therefore, it is critical that the analysis of microglial
40 engulfment of cellular and protein substrates is performed with the highest rigor.

41 Confocal light microscopy has become a standard method to measure microglial
42 engulfment function in tissues and cells[10,11]. A potential confound of these studies is
43 autofluorescence (AF) in brain tissue. Likely the largest source of AF in tissues is lipofuscin.
44 Lipofuscin is a mixture of highly oxidized lipids, misfolded proteins, and metals, which
45 accumulates with age within lysosomal compartments[12-14]. These lipofuscin aggregates
46 autofluoresce across the fluorescent spectrum, making it challenging to image fluorescently
47 labeled cells and molecules by light microscopy[15,16,17,18]. In microglia, the aggregation of lipofuscin
48 can be induced by incomplete myelin digestion and disruption of the lysosomal pathway, which
49 implicates phagocytosis of cellular material as a key mechanism leading to lipofuscin buildup[19].
50 Further, lipofuscin accumulation in microglia is an age-dependent process and it has been
51 estimated that AF-positive microglia, which is likely lipofuscin, outnumber AF-negative microglia
52 by greater than two-fold in 6-month-old mice[17,20]. However, recently AF attributed to lipofuscin has
53 been shown within microglia lysosomes as early as 7–9 weeks[17,18]. Thus, it is important to
54 consider the potential confound that lipofuscin in microglia can be misinterpreted as engulfed

bioRxiv preprint doi: https://doi.org/10.1101/2023.02.28.530224; this version posted March 1, 2023. The copyright holder for this preprint (which was not certified by peer review) is the author/funder, who has granted bioRxiv a license to display the preprint in perpetuity. It is made available under aCC-BY 4.0 International license.

55 cellular and protein material by microglia, leading to false positive detection of engulfed material
56 within microglia.

57 Here, we assessed AF, which is likely from lipofuscin (lipofuscin-like AF or lipo-AF), within
58 microglia using confocal light microscopy across the developing, adult, aged and diseased mouse
59 cortex. Our data show that microglia are the first resident CNS cell type to accumulate lipo-AF,
60 with a small amount of AF detected within microglia in the postnatal and juvenile mouse cortex.
61 We also provide evidence that, if not taken into consideration, lipo-AF can potentially be
62 misinterpreted as engulfed material within microglia, even in the young adult brain. Finally, we
63 provide an adaptable pre-staining AF quenching protocol that preserves immunofluorescent
64 antibody signal. This protocol can further be applied across species, including mouse, marmoset,
65 and human brain tissue.

66 **Results**

67 **Lipofuscin-like autofluorescence accumulates within microglial lysosomes with age**
68 **independent of neurodegeneration**

69 We began imaging tissue at postnatal day 90 (P90) when other studies have shown a
70 significant accumulation of AF, likely due to lipofuscin, within microglia in the mouse brain by light
71 microscopy[17,18,21]. We focused our imaging in the somatosensory cortex and neighboring visual
72 and auditory cortices as this was a large region that could be easily identified across ages and is
73 known to undergo neurodegeneration (Fig. 1). Unstained tissue (Fig. 1a-b) or tissue
74 immunostained to label microglia (anti-IBA1) were imaged (Fig. 1d-e). The AF signal within the
75 unstained cortex at P90 was observed with a 488 nm laser (Green, Band Pass Filter (BP) 525/50),
76 561nm laser (Red; BP 629/62), and 638nm laser (Far-red; BP 690/50), but not the 350 nm laser
77 (Blue, BP 450/50) (Fig. 1b,c). Further, when assessed within anti-IBA1 immunostained tissue,
78 this AF was largely localized to CD68+ lysosomes (Supplementary Fig. 1). Because of these

bioRxiv preprint doi: https://doi.org/10.1101/2023.02.28.530224; this version posted March 1, 2023. The copyright holder for this preprint (which was not certified by peer review) is the author/funder, who has granted bioRxiv a license to display the preprint in perpetuity. It is made available under aCC-BY 4.0 International license.

79 excitation and emission properties of the AF signal and the localization of the AF signal within
80 lysosomes, it is most likely due to lipofuscin[13,16,18,21-23]. Other AF molecules generally have a
81 tighter excitation and emission spectra and are not localized specifically to lysosomal
82 compartments[23]. However, there does not exist a highly specific stain for lipofuscin, therefore, we
83 refer to it as lipofuscin-like AF or lipo-AF.

84 We then extended our analyses to earlier developmental timepoints and assessed the
85 liop-AF within anti-IBA-1 immunostained tissue (Fig. 1d-k). For simplicity, we continued our
86 analyses using the 561nm laser (BP 629/62). From P5 to P30, most microglia had low to no
87 detectable lipo-AF within their cytoplasm (0–0.1% of microglia volume) (Fig. 1f (dark blue) and g).
88 However, there was a subset of microglia at these early ages (P5=24.5%±7%, P15=8.9%±3.4,
89 P30= 17.9%±6.2) that contained more lipo-AF within their cytoplasm (Fig. 1f (light blue and pink)
90 and h-i). By P60, there was a significant increase of lipo-AF within microglia compared to younger
91 ages with 54.2%±13.4 of the total microglia with >0.1–1% of their volume occupied by lipo-AF
92 (Fig. 1f (light blue) and h). This was further increased to 76.9%±0.9 of microglia with >0.1–1% of
93 their volume occupied by lipo-AF by P90 (Fig. 1f (light blue) and 1h). As expected, most microglia
94 (87.3%±7.2) from aged, 24-month-old brain had >2.0% of their volume occupied by lipo-AF (Fig.
95 1f (dark red) and j). Interestingly, lipo-AF was largely localized within microglia in the young adult
96 brain, but by 24 months, a significantly higher percentage of lipo-AF was localized outside
97 microglia (Fig. 1e,k).

98 Increased microglial engulfment of cellular material and protein aggregates has also been
99 shown in the context of neurodegeneration, and microglial engulfment of myelin has been
100 suggested to drive the accumulation of lipo-AF in microglia[12,19]. We, therefore, next assessed
101 microglial AF accumulation in an Alzheimer's disease (AD)-relevant mouse model, the 5XFAD
102 model (Fig. 2). Surprisingly, while AF was observed in microglia in the somatosensory cortex of
103 9-month-old 5XFAD mice, it was comparable to 9-month wild-type (WT) controls (Fig. 2c-g).

bioRxiv preprint doi: https://doi.org/10.1101/2023.02.28.530224; this version posted March 1, 2023. The copyright holder for this preprint (which was not certified by peer review) is the author/funder, who has granted bioRxiv a license to display the preprint in perpetuity. It is made available under aCC-BY 4.0 International license.

104 Moreover, in Aβ plaque-enriched cortical regions, a significantly higher percentage of microglia
105 had little to no detectable lipo-AF (0–0.1%) within their cytoplasm compared to WT mice or non-
106 plaque-associated microglia in 5XFAD mice (Fig. 2c, dark blue and d).

107 Together, these data demonstrate that microglia accumulate lipo-AF prior to other cell
108 types and earlier than previously appreciated. While lipo-AF accumulates inside and outside
109 microglia with age, there does not appear to be a significant increase in lipo-AF accumulation
110 within cortical microglia in the presence of Aβ plaques in 5XFAD mice.

111 **A reliable protocol to quench lipo-AF in mouse brain tissue**

112 Considering the potential for lipo-AF to confound downstream analyses, we explored
113 protocols to reduce microglial AF in brain tissue. Previous groups have used a commercially
114 available derivative of Sudan Black to eliminate AF in tissues[18]. We repeated these experiments
115 at P90, a timepoint when lipo-AF accumulation in microglia is significantly increased (Fig. 1).
116 Using the commercially available reagent TrueBlack Plus™ after immunostaining, we then
117 imaged with a 561nm laser (BP 629/62) and identified a significant decrease in microglial lipo-AF
118 (Fig. 3a-f). That is, with quenching, there was a significant decrease in microglia with detectable
119 lipo-AF (>0.1–2%) (Fig. 3c light blue, pink and e-f) and a significant increase in microglia with
120 negligible to low lipo-AF (0–0.1%, Fig. 3c dark blue and d). However, this TrueBlack Plus™
121 quenching protocol also resulted in a significant decrease in the intensity of an immunostained
122 protein of interest in the tissue (anti-P2RY12; Fig. 3b, g). Therefore, we took steps to improve this
123 methodology using a commercially available MERSCOPE photobleacher device typically used
124 for multiplexed error-robust fluorescence in situ hybridization (MERFISH). This device uses light
125 to photobleach samples prior to immunostaining. Other groups have used LED light-based
126 systems to achieve similar effects in tissues[21,24]. After incubating mouse brain sections in
127 photobleaching light for 12 hours, we proceeded with our standard immunostaining protocol (Fig.

bioRxiv preprint doi: https://doi.org/10.1101/2023.02.28.530224; this version posted March 1, 2023. The copyright holder for this preprint (which was not certified by peer review) is the author/funder, who has granted bioRxiv a license to display the preprint in perpetuity. It is made available under aCC-BY 4.0 International license.

128 3h). In contrast to chemical quenching methods (Fig. 3a-g), this photobleaching method
129 significantly eliminated lipo-AF signal within P90 cortical microglia (Fig. 3i-m) without
130 compromising the fluorescent signal of anti-P2RY12+ immunostaining (Fig. 3i,n).

131 **Photobleaching can be used to eliminate lipo-AF signal prior to microglial engulfment**
132 **analyses**

133 Given that lipo-AF is localized within microglial lysosomes (Supplementary Fig. 1), it is
134 possible that it could confound assessments of engulfed cellular material within microglia. As
135 synapses are key phagocytic substrates for microglia in health and disease[1-4], we used our
136 photobleaching protocol to next determine the impact of lipo-AF on microglial synapse engulfment
137 analysis. Beginning with P90 mouse brain, sections were immunostained for anti-IBA1 to label
138 microglia and anti-vesicular glutamate transporter 2 (VGluT2) to label excitatory presynaptic
139 terminals in layer IV of the somatosensory cortex (Fig. 4a). Neighboring sections from the same
140 brain were left unstained to measure lipo-AF in the same region. A 561nm laser (BP 629/62) was
141 used to image lipo-AF and anti-VGluT2 signal. The intensity of the anti-VGluT2 immunolabelled
142 puncta outside and inside the microglial boundaries, as well as lipo-AF in the neighboring
143 sections, were measured in resulting images (Fig. 4b, immunostained sections are shown).
144 Notably, at P90, the anti-VGluT2 puncta intensity inside the microglia (Fig. 4b,c orange bar) was
145 not significantly different from the lipo-AF intensity captured with the same settings and the same
146 laser line (Fig. 4c gray bar). This suggests that, with the 561 nm laser line (BP 629/62), lipo-AF
147 can yield a comparable signal to anti-VGluT2 immunostaining within microglia and raises the
148 possibility that this can confound analysis of engulfed material within microglia.

149 We more directly tested the extent to which the anti-VGluT2 signal detected within the
150 microglial boundaries could be confounded by lipo-AF signal using the photobleaching protocol
151 (Fig. 3h). We first photobleached P90 tissue to rid of AF and then immunostained tissue for

bioRxiv preprint doi: https://doi.org/10.1101/2023.02.28.530224; this version posted March 1, 2023. The copyright holder for this preprint (which was not certified by peer review) is the author/funder, who has granted bioRxiv a license to display the preprint in perpetuity. It is made available under aCC-BY 4.0 International license.

152 VGluT2 and IBA1. We imaged all tissues with a 561nm laser (BP 629/62) in the P90 and P5
153 mouse somatosensory cortex. We chose to compare P90 to P5 as P5 was a developmental
154 timepoint where lipo-AF was low (Fig. 1), and it is an age where the somatosensory cortex is
155 known to undergo extensive experience-dependent synapse remodeling by phagocytic
156 microglia[25]. In untreated sections, apparent engulfed VGluT2 material was detectable within
157 microglia at P5 and P90 (Fig. 4d-e). However, after photobleaching, this engulfed VGluT2 signal
158 was no longer detected at P90 (Fig. 4d,f). In contrast, microglia within the P5 cortex displayed
159 similar levels of engulfed VGluT2+ material within their cytosol in the photobleached and non-
160 photobleached condition (Fig. 4e-f). We further compared the fold difference in signal intensity of
161 anti-VGluT2 signal within microglia after photobleaching to without photobleaching (post-
162 photobleaching anti-VGluT2+ signal within microglia/pre-photobleaching signal). There was a
163 significant reduction in anti-VGluT2 within microglia in the P90 cortex after photobleaching
164 compared to P5 (Fig. 4f). Together, these data suggest that lipo-AF can confound the
165 interpretation of fluorescent signal within microglial lysosomes in young adult mouse brain tissue,
166 but this is less of a concern in neonate brain tissue. Nonetheless, precautions should be taken to
167 eliminate lipo-AF to avoid false positive detection of engulfment events.

168 **Photobleaching eliminates autofluorescence in aged mouse, marmoset, and human brain**
169 **tissue**

170 Photobleaching effectively quenched lipo-AF in mouse tissue (Figs. 3-4). We, thus,
171 extended this protocol to older mouse tissue and to other species (Fig. 5). We found that
172 extending the photobleaching period to 24 hours significantly reduced AF signal across multiple
173 fluorescence channels in 24-month-old aged mouse cortex (Fig. 5a,e) and 9-month-old 5xFAD
174 mouse cortex (Fig. 5b, f). Similar to our experiments in mice, we found that photobleaching for 24
175 hours significantly reduced the signal intensity from AF across multiple fluorescence channels in
176 formalin-fixed, paraffin-embedded (FFPE) 11–13 year-old marmoset cortex (Fig. 5c,g) and FFPE

bioRxiv preprint doi: https://doi.org/10.1101/2023.02.28.530224; this version posted March 1, 2023. The copyright holder for this preprint (which was not certified by peer review) is the author/funder, who has granted bioRxiv a license to display the preprint in perpetuity. It is made available under aCC-BY 4.0 International license.

177 60–77 year-old human cortex (Fig. 5d,h). Note, the human tissue was collected from the
178 postmortem brains of multiple sclerosis (MS) subjects. Together, we have implemented a new
179 pre-staining protocol that reliably eliminates AF in tissue sections in different tissue preparations.
180 As this protocol can be adapted for multiple species tissues, including human, the protocol has
181 broad applicability.

182 Discussion

183 Here, we assessed microglia-associated lipo-AF in the developing, adult, aged, and
184 diseased mouse cortex using confocal light microscopy. A small degree of microglial lipo-AF could
185 be detected as early as P5 and microglia were the first cells in the mouse cortex to accumulate
186 lipo-AF. Lipo-AF within microglia increased into adulthood and a large accumulation of lipo-AF
187 was detected inside and outside of microglia in the aged mouse cortex. We further showed that
188 lipo-AF within microglia can be mis-interpreted as engulfed synaptic material, particularly in the
189 young adult mouse brain. Finally, we provide a new protocol to rid tissues of AF signal before
190 immunostaining to reduce the confound of lipo-AF for microglial engulfment studies, which can
191 also be applied to any other study reliant on fluorescence light microscopy. Importantly, we show
192 that this AF quenching protocol is broadly applicable and can be performed in mouse, non-human
193 primate, and human brain tissues.

194 One surprising result from this study is that neurodegeneration and Aβ accumulation in
195 5XFAD mice did not exacerbate the accumulation of lipo-AF in microglia. One study has found
196 that, following microglia depletion, the proliferating microglia were primarily restricted to the AF-
197 negative, likely lipofuscin-negative, subset of cells[17]. It is also known that cell division is the only
198 way cells can reduce lipofuscin, which is likely to underlie the lipo-AF signal we are observing in
199 brain tissue[13,14,22]. That is, as cells divide, lipofuscin is diluted. Thus, it is possible that lipofuscin-
200 negative microglia or microglia with low amounts of lipofuscin proliferate during
201 neurodegeneration and, thus, the amount of lipofuscin and AF due to lipofuscin per cell is

bioRxiv preprint doi: https://doi.org/10.1101/2023.02.28.530224; this version posted March 1, 2023. The copyright holder for this preprint (which was not certified by peer review) is the author/funder, who has granted bioRxiv a license to display the preprint in perpetuity. It is made available under aCC-BY 4.0 International license.

202 decreased. Indeed, it has been previously shown in 5XFAD mice that cortical microglia increase,
203 and microglia near Aβ plaques proliferate[26,27]. It is also possible that lipo-AF accumulation is
204 disease and/or substrate specific. For example, the engulfment of myelin in a demyelinating
205 disease related to MS has been suggested to drive lipofuscin accumulation in microglia[19].
206 Therefore, specific engulfed substrates may lead to the accumulation of lipofuscin, while others
207 do not. An important future direction will be to understand the prevalence of this biology in
208 microglia across different diseases.

209 What is the source of lipo-AF, and how does it accumulate in microglia? We speculate
210 that the broad phagocytic role of microglia in early development may explain the presence of the
211 small amount of lipo-AF within microglia in the early postnatal cortex. This lipo-AF is likely from
212 lipofuscin given its excitation and emission spectra. It is possible that the lysosomal degradation
213 capacity of microglia in the young brain may be able to compensate and/or microglia are actively
214 dividing in the young brain and, thereby, lipofuscin is being diluted. In contrast, during adulthood,
215 ongoing engulfment of cellular material and decreased cell division may lead to accumulation of
216 lipofuscin and its related AF. This may also increase with aging as a result of age-related
217 lysosomal dysfunction[12]. Indeed, recent studies have shown how disruption of the lysosomal
218 degradation pathway in microglia during engulfment can contribute to lipofuscin accumulation[19].
219 Better defining the molecular composition and accumulation of these lipo-AF deposits in microglia
220 throughout the lifespan and disease would be most informative.[17, 19]

221 Another important aspect of our study is that we provide two distinct methods to eliminate
222 AF signal from tissue sections before imaging. The first uses the commercially available reagent
223 TrueBlack Plus™, an alternative to Sudan Black dye. Our data shows that a 15-minute post-
224 staining treatment was sufficient to eliminate the AF signal. However, we also found a significant
225 quenching of the immunostained fluorophore signal. The second method consisted of incubating
226 sections in a commercially available device that administers light to a sample for an extended

bioRxiv preprint doi: https://doi.org/10.1101/2023.02.28.530224; this version posted March 1, 2023. The copyright holder for this preprint (which was not certified by peer review) is the author/funder, who has granted bioRxiv a license to display the preprint in perpetuity. It is made available under aCC-BY 4.0 International license.

227 period. Using this device, we found that photobleaching brain tissue sections with light for 12-24
228 hours significantly reduces the AF signal without compromising fluorophore signal intensity. While
229 our device's intensity and wavelength of light remains proprietary, previous studies have used a
230 similar photobleaching strategy with LEDs[24, 21,28]. Thus, this technology could be easily adapted
231 across laboratories and tissue samples. Finally, we applied the photobleaching protocol in the
232 context of microglial synapse engulfment analysis[10]. Several studies have shown how microglia
233 engulf synaptic material at neonatal time points[1,3,4]. Despite detecting low levels of microglial lipo-
234 AF in the early postnatal P5 brain, it had no confounding effect on the analysis of VGluT2
235 engulfment within microglia. That is, anti-VGluT2 immunofluorescence signal was still observed
236 within microglia after photobleaching samples. Conversely, in young, adult mice (P90), apparent
237 engulfed VGluT2 within microglia was no longer observed after photobleaching. Therefore,
238 caution should be used when interpreting microglial engulfment, particularly in adult mouse brain.
239 It is noted that, although we detected lipo-AF with 3 different laser lines (Fig. 1), we did most of
240 our analyses with the 561nm laser (BP 629/62). There may be variations in detecting lipo-AF on
241 other microscope set ups and with other laser lines and filter sets. Still, photobleaching samples
242 before immunostaining and including secondary-only controls to evaluate the amount of
243 lipofuscin-derived AF or other sources of AF in tissue sections are the best practice. This is
244 particularly important considering that engulfed material and lipo-AF share the same subcellular
245 compartment (i.e., lysosomes) within microglia.

246 In summary, as more and more studies are realizing the impact of microglial engulfment
247 mechanisms on neural circuit structure and function[1-4], it is critical to perform experiments to
248 assess engulfment of cellular and protein substrates by microglia to the highest rigor. The
249 protocols we provide ensure that microglial engulfment confocal imaging assays are not
250 confounded by AF. Importantly, these protocols can be used in mouse models, but the protocols
251 can also be adapted for use in non-human primate and human tissue samples.

bioRxiv preprint doi: https://doi.org/10.1101/2023.02.28.530224; this version posted March 1, 2023. The copyright holder for this preprint (which was not certified by peer review) is the author/funder, who has granted bioRxiv a license to display the preprint in perpetuity. It is made available under aCC-BY 4.0 International license.

252 **Materials and Methods**

253 **Animals.** Male and female wildtype C57Bl/6J mice (stock #000664) were obtained from Jackson
254 Laboratories (Bar Harbor, ME). Adult common marmosets (*Callithrix jacchus*), both male and
255 females between 11-13 years old, were obtained from the marmoset tissue library of translational
256 neuroradiology section (TNS) at the NINDS. All animal experiments were performed in
257 accordance with Animal Care and Use Committees (IACUC) and under NIH guidelines for proper
258 animal welfare.

259 **Human samples.** Collection of human multiple sclerosis (MS) postmortem brain tissue was
260 performed after obtaining informed consent for collection and were obtained from the
261 Translational Neuroradiology Section at the NIH/NINDS. Samples analyzed in the current study
262 were collected from the insular/parietal neocortex and prefrontal cortex of 3 women with multiple
263 sclerosis (MS) with ages ranging from 60–77 years.

264 **Immunostaining.** Mice were anesthetized and transcardially perfused with 0.1M phosphate
265 buffer (PB) followed by 4% paraformaldehyde (PFA) (Electron Microscopy Services 15710)/0.1M
266 PB. Brains were post-fixed at 4°C in PFA overnight, equilibrated in 30% sucrose/0.1M PB and
267 then embedded in a 2:1 mixture of 30% sucrose/0.1M PB and O.C.T. compound (ThermoFisher
268 Scientific Waltham, MA, USA). To ensure methods were of global use, sections were
269 immunostained on slides or floating. A cryostat was used to cut either 10-16 μm coronal brain
270 sections on slides (microglial lipo-AF analysis across development and in 5XFAD mice) or 40 μm
271 floating sections in 0.1M PB (lipo-AF intensity, quenching and synaptic engulfment analysis).
272 Subsequent sections were blocked and permeabilized at room temperature for 1 hr in blocking
273 solution (10% normal goat serum/0.1M PB containing 0.3% Triton-X 100) followed by overnight
274 incubation with primary antibodies at ambient room temperature. Primary antibodies included: Rat
275 mAb anti-CD68 (Abcam, ab955; 1:200), rabbit pAb anti-IBA1 (Wako Chemicals, 019-19741;

bioRxiv preprint doi: https://doi.org/10.1101/2023.02.28.530224; this version posted March 1, 2023. The copyright holder for this preprint (which was not certified by peer review) is the author/funder, who has granted bioRxiv a license to display the preprint in perpetuity. It is made available under aCC-BY 4.0 International license.

276 1:500), chicken mAb anti-IBA1 (Synaptic Systems, 234009; 1:500), rabbit pAb anti-P2RY12
277 (Anaspec, 55043A; 1:2000) and guinea pig pAb anti-VGluT2 (Millipore, Ab2251-I; 1:1000). The
278 following day, sections were washed 3x5 min with 0.1M PB and incubated with the appropriate
279 Alexa-fluorophore-conjugated secondary antibodies including goat anti-chicken IgY (H+L) Alexa-
280 Fluor 488 IgY (Life Technologies Scientific; A11039), goat anti-rabbit IgG (H+L) Alexa-Fluor 488
281 (Life Technologies; A11034), goat anti-guinea pig IgG (H+L) Alexa-Fluor 488 (Life Technologies;
282 A11073), goat anti-rabbit IgG (H+L) Alexa-Fluor 594 (Life Technologies; A11012), goat anti-
283 guinea pig IgG (H+L) Alexa-Fluor 594 (Life Technologies; A11076), goat anti-rabbit IgG (H+L)
284 Alexa-Fluor 647 (Life Technologies; A21245), goat anti-guinea pig IgG (H+L) Alexa-Fluor 647
285 (Life Technologies; A21450), goat anti-rat IgG (H+L) Alexa-Fluor 647 (Life Technologies; A21247)
286 for 2 hr at room temperature. Slides and floating sections were washed 3x10 min with 0.1M PB.
287 Floating sections were then mounted on slides. All subsequent slides were air dried and cover
288 glass (ThermoFisher; 12-544-DP) was mounted with Vectashield containing DAPI (Vector
289 laboratories, Burlingame, CA, USA) or with CFM-3 (Citifluor, Hatfield, PA, USA) for chemical
290 quenching experiments.

291 **Chemical quenching.** After staining, floating sections or tissue-mounted slides were incubated
292 with TrueBlack® Plus Lipofuscin Autofluorescence Quencher (Biotium, Fremont, CA, USA) in 1X
293 phosphate buffer saline (PBS) for 15 min at room temperature with rocking. Following 3x5 min
294 washes with PBS 1X, sections were mounted with CFM-3 (Citifluor, Hatfield, PA, USA).

295 **Photobleaching.** Before incubating in blocking solution, floating sections or tissue-mounted
296 slides were placed in 0.1M PB and incubated in the MERSCOPE Photobleacher (Vizgen,
297 Cambridge, MA, USA) for 12-24 hour. Photobleached samples were then incubated in blocking
298 solution and immunostained as described above.

bioRxiv preprint doi: https://doi.org/10.1101/2023.02.28.530224; this version posted March 1, 2023. The copyright holder for this preprint (which was not certified by peer review) is the author/funder, who has granted bioRxiv a license to display the preprint in perpetuity. It is made available under aCC-BY 4.0 International license.

299 **Confocal Imaging.** Mounted brain sections were imaged using Zen Blue acquisition software
300 (Zeiss; Oberkochen, Germany) on a Zeiss Observer Spinning Disk confocal microscope equipped
301 with diode lasers 405 nm/50 mW, 488 nm/50 mW, 561 nm/50 mW, and 638 nm/75 mW, and with
302 450/50 (blue), 525/50 (green), 629/62 (red) and 690/50 (far-red) BP emission filter sets,
303 respectively. For most experiments, 6-12 (AF) or 3 (anti-VGluT2 immunostained sections) 40x
304 fields of view were randomly chosen within the somatosensory and neighboring visual and
305 auditory cortices an z-stacks were acquired at 0.31 μm spacing. For AF, anti-VGluT2, and anti-
306 P2RY12 intensity measurements, 2-4 63x fields of view were randomly and z-stacks were then
307 acquired at 0.27 μm spacing. For all imaging experiments, identical settings were used to acquire
308 images from all samples within one experiment.

309 **Quantification of lipo-AF and VGluT2 volume.** Images were first pre-processed and blinded
310 using a custom macro in ImageJ (NIH, version 1.53c). Imaris v9 (Bitplane) was then used to
311 create a 3D surface rendering of single microglia cells. A 3D surface rendering of masked anti-
312 CD68+ signal from each cell was also created and was used to generate a 3D surface rendering
313 of CD68-masked AF+ or CD68-masked VGluT2+ material. Lipo-AF or VGluT2 within microglia
314 was calculated by dividing the volume of CD68-masked lipo-AF or VGluT2 by the volume of the
315 individual microglial cell. To quantify lipo-AF or VGluT2 signal outside the microglia volume, a 3D
316 surface rendering of total lipo-AF or VGlut2 was created and the volume of lipo-AF or VGluT2
317 within microglia was then subtracted.

318 **Quantification of VGluT2 and lipo-AF signal intensity.** All analyses of intensity were performed
319 on single z-planes blind to condition using ImageJ (NIH, version 1.53c). Briefly, for sections
320 stained with anti-VGluT2 and anti-IBA1, square regions of interests (ROIs) of equal size were
321 drawn at the center of anti-IBA1 immunolabelled microglial somas containing anti-VGluT2 positive
322 signal. Within these ROIs, smaller circular ROIs of equal size were placed at the center of anti-
323 VGluT2 immunolabelled puncta outside and inside anti-IBA1 immunolabelled microglia. Three

bioRxiv preprint doi: https://doi.org/10.1101/2023.02.28.530224; this version posted March 1, 2023. The copyright holder for this preprint (which was not certified by peer review) is the author/funder, who has granted bioRxiv a license to display the preprint in perpetuity. It is made available under aCC-BY 4.0 International license.

324 background circular ROIs of the same size were also selected for each field of view within the
325 single z-plane. The raw integrated density of pixels within each circular ROI was measured. To
326 quantify lipo-AF intensity, unstained sections were imaged and subsequently ROIs of equal size
327 were drawn at the center of single z-planes containing multiple lipo-AF puncta. Similar to
328 immunostained sections, circular ROIs of equal size were then placed at the center of AF. Three
329 background ROIs were also selected. For all images (immunostained with VGluT2 or unstained
330 to measure AF), the raw integrated density of pixels within each circular ROI was measured and
331 the background ROI pixel intensity value was averaged. Last, for each VGluT+ or AF+ puncta
332 intensity measurement, the average background was subtracted prior to statistical comparison.

333 **Quantification of P2Y12R signal intensity.** To quantify the fluorescence intensity of anti-
334 P2Y12R signal, Imaris v9 (Bitplane) was used to create a 3D surface rendering of all microglia
335 cells and the intensity mean parameter of anti-P2Y12R signal was then extracted.

336 **Quantification of AF signal intensity after photobleaching in mouse, marmoset, and human**
337 **brain tissue.** Unstained sections were imaged on a Zeiss Observer Spinning Disk confocal
338 microscope as described above. All subsequent analyses of intensity were performed on single
339 z-planes using ImageJ (NIH, version 1.53c). For each image, the 488 nm laser channel was
340 background subtracted (10x) and despeckled (median filter, 3x3) in ImageJ and was then ROIs
341 were selected using the analyze particle function. These ROIs were then applied across all
342 channels for that image. The raw integrated density of pixels within each individual ROI was then
343 measured for each fluorescence channel. The average raw integrated density of pixels for each
344 of three z-stacks was then calculated, and the average per biological replicate and condition were
345 calculated.

346 **Statistical analysis.** Results are presented as either mean or mean ± standard error (SEM). For
347 normally distributed data, analyses included two-tailed, unpaired Students t-test when comparing

bioRxiv preprint doi: https://doi.org/10.1101/2023.02.28.530224; this version posted March 1, 2023. The copyright holder for this preprint (which was not certified by peer review) is the author/funder, who has granted bioRxiv a license to display the preprint in perpetuity. It is made available under aCC-BY 4.0 International license.

348 2 conditions or one-way ANOVA followed by Tukey's post hoc analysis or two-way ANOVA
349 followed by Sidak's post hoc analyses (indicated in figure legends) using GraphPad Prism (La
350 Jolla, CA). For data that were not normally distributed, a Mann-Whitney test was used. Values of
351 $*p < 0.05$, $**P < 0.01$, $***P < 0.001$, $****P < 0.0001$ were considered statistically significant.
352
353

bioRxiv preprint doi: https://doi.org/10.1101/2023.02.28.530224; this version posted March 1, 2023. The copyright holder for this preprint (which was not certified by peer review) is the author/funder, who has granted bioRxiv a license to display the preprint in perpetuity. It is made available under aCC-BY 4.0 International license.

354 **Acknowledgments**

355 We thank Dr. Christina Baer (UMMS) for critical reading of the manuscript and assistance with
356 microscopy. We thank Joan Ohayon, CRNP, for coordinating MS autopsies. This work was
357 supported by NIMH-R01MH113743 (DPS), NINDS-R01NS117533 (DPS), NIA-RF1AG068281
358 (DPS), NIH-T32AI132152 (JMS), the Intramural Research Program of NINDS (DSR), and the Dr.
359 Miriam and Sheldon G. Adelson Medical Research Foundation (DPS and DSR).

360 **Author contributions**

361 J.M.S., F.M.L, and D.P.S. designed the study and wrote the manuscript. J.M.S., F.M.L, and D.P.S.
362 performed and analyzed the experiments. D.S.R. supervised collection and processing of
363 marmoset and human brain tissue by J.L. and K.H. All authors edited and revised the manuscript.

364 **Competing interests**

365 No competing interests.

366 **Materials & Correspondence**

367 All materials and correspondences should be addressed to Dr. Dorothy P. Schafer
368 dorothy.schafer@umassmed.edu.

369

370

371

372

373

374

375

376

bioRxiv preprint doi: https://doi.org/10.1101/2023.02.28.530224; this version posted March 1, 2023. The copyright holder for this preprint (which was not certified by peer review) is the author/funder, who has granted bioRxiv a license to display the preprint in perpetuity. It is made available under aCC-BY 4.0 International license.

377 **References**

378 1 Schafer, D. P. & Stevens, B. Phagocytic glial cells: sculpting synaptic circuits in the
379 developing nervous system. *Current opinion in neurobiology* **23**, 1034-1040,
380 doi:10.1016/j.conb.2013.09.012 (2013).
381 2 Hong, S., Dissing-Olesen, L. & Stevens, B. New insights on the role of microglia in synaptic
382 pruning in health and disease. *Current opinion in neurobiology* **36**, 128-134,
383 doi:10.1016/j.conb.2015.12.004 (2016).
384 3 Stevens, B. & Schafer, D. P. Roles of microglia in nervous system development, plasticity,
385 and disease. *Dev Neurobiol* **78**, 559-560, doi:10.1002/dneu.22594 (2018).
386 4 Faust, T. E., Gunner, G. & Schafer, D. P. Mechanisms governing activity-dependent
387 synaptic pruning in the developing mammalian CNS. *Nature reviews. Neuroscience* **22**,
388 657-673, doi:10.1038/s41583-021-00507-y (2021).
389 5 Crapser, J. D., Arreola, M. A., Tsourmas, K. I. & Green, K. N. Microglia as hackers of the
390 matrix: sculpting synapses and the extracellular space. *Cell Mol Immunol* **18**, 2472-2488,
391 doi:10.1038/s41423-021-00751-3 (2021).
392 6 Song, W. M. & Colonna, M. The identity and function of microglia in neurodegeneration.
393 *Nat Immunol* **19**, 1048-1058, doi:10.1038/s41590-018-0212-1 (2018).
394 7 Germann, M., Brederoo, S. G. & Sommer, I. E. C. Abnormal synaptic pruning during
395 adolescence underlying the development of psychotic disorders. *Curr Opin Psychiatry* **34**,
396 222-227, doi:10.1097/YCO.0000000000000696 (2021).
397 8 Biber, K., Moller, T., Boddeke, E. & Prinz, M. Central nervous system myeloid cells as
398 drug targets: current status and translational challenges. *Nature reviews. Drug discovery*
399 **15**, 110-124, doi:10.1038/nrd.2015.14 (2016).
400 9 Priller, J. & Prinz, M. Targeting microglia in brain disorders. *Science* **365**, 32-33,
401 doi:10.1126/science.aau9100 (2019).
402 10 Schafer, D. P., Lehrman, E. K., Heller, C. T. & Stevens, B. An engulfment assay: a protocol
403 to assess interactions between CNS phagocytes and neurons. *Journal of visualized*
404 *experiments : JoVE*, doi:10.3791/51482 (2014).
405 11 Morini, R., Bizzotto, M., Perrucci, F., Filipello, F. & Matteoli, M. Strategies and Tools for
406 Studying Microglial-Mediated Synapse Elimination and Refinement. *Front Immunol* **12**,
407 640937, doi:10.3389/fimmu.2021.640937 (2021).
408 12 Moreno-Garcia, A., Kun, A., Calero, O., Medina, M. & Calero, M. An Overview of the Role
409 of Lipofuscin in Age-Related Neurodegeneration. *Front Neurosci* **12**, 464,
410 doi:10.3389/fnins.2018.00464 (2018).
411 13 Brunk, U. T. & Terman, A. Lipofuscin: mechanisms of age-related accumulation and
412 influence on cell function. *Free Radic Biol Med* **33**, 611-619, doi:10.1016/s0891-
413 5849(02)00959-0 (2002).
414 14 Gray, D. A. & Woulfe, J. Lipofuscin and aging: a matter of toxic waste. *Sci Aging*
415 *Knowledge Environ* **2005**, re1, doi:10.1126/sageke.2005.5.re1 (2005).
416 15 Calin, E. F. *et al.* Lipofuscin: a key compound in ophthalmic practice. *Rom J Ophthalmol*
417 **65**, 109-113, doi:10.22336/rjo.2021.23 (2021).
418 16 Mochizuki, Y., Park, M. K., Mori, T. & Kawashima, S. The difference in autofluorescence
419 features of lipofuscin between brain and adrenal. *Zoolog Sci* **12**, 283-288,
420 doi:10.2108/zsj.12.283 (1995).
421 17 Burns, J. C. *et al.* Differential accumulation of storage bodies with aging defines discrete
422 subsets of microglia in the healthy brain. *Elife* **9**, doi:10.7554/eLife.57495 (2020).
423 18 Zhang, H., Tan, C., Shi, X. & Xu, J. Impacts of autofluorescence on fluorescence based
424 techniques to study microglia. *BMC Neurosci* **23**, 21, doi:10.1186/s12868-022-00703-1
425 (2022).

bioRxiv preprint doi: https://doi.org/10.1101/2023.02.28.530224; this version posted March 1, 2023. The copyright holder for this preprint (which was not certified by peer review) is the author/funder, who has granted bioRxiv a license to display the preprint in perpetuity. It is made available under aCC-BY 4.0 International license.

426 19 Safaiyan, S. *et al.* Age-related myelin degradation burdens the clearance function of
427 microglia during aging. *Nat Neurosci* **19**, 995-998, doi:10.1038/nn.4325 (2016).
428 20 Sierra, A., Gottfried-Blackmore, A. C., McEwen, B. S. & Bulloch, K. Microglia derived from
429 aging mice exhibit an altered inflammatory profile. *Glia* **55**, 412-424,
430 doi:10.1002/glia.20468 (2007).
431 21 Tsuneoka, Y., Atsumi, Y., Makanae, A., Yashiro, M. & Funato, H. Fluorescence quenching
432 by high-power LEDs for highly sensitive fluorescence in situ hybridization. *Frontiers in*
433 *molecular neuroscience* **15**, 976349, doi:10.3389/fnmol.2022.976349 (2022).
434 22 Terman, A. & Brunk, U. T. Lipofuscin: mechanisms of formation and increase with age.
435 *APMIS* **106**, 265-276, doi:10.1111/j.1699-0463.1998.tb01346.x (1998).
436 23 Croce, A. C. & Bottiroli, G. Autofluorescence spectroscopy and imaging: a tool for
437 biomedical research and diagnosis. *Eur J Histochem* **58**, 2461, doi:10.4081/ejh.2014.2461
438 (2014).
439 24 Duong, H. & Han, M. A multispectral LED array for the reduction of background
440 autofluorescence in brain tissue. *J Neurosci Methods* **220**, 46-54,
441 doi:10.1016/j.jneumeth.2013.08.018 (2013).
442 25 Gunner, G. *et al.* Sensory lesioning induces microglial synapse elimination via ADAM10
443 and fractalkine signaling. *Nature neuroscience* **22**, 1075-1088, doi:10.1038/s41593-019-
444 0419-y (2019).
445 26 Forner, S. *et al.* Systematic phenotyping and characterization of the 5xFAD mouse model
446 of Alzheimer's disease. *Sci Data* **8**, 270, doi:10.1038/s41597-021-01054-y (2021).
447 27 Wang, Y. *et al.* TREM2-mediated early microglial response limits diffusion and toxicity of
448 amyloid plaques. *The Journal of experimental medicine* **213**, 667-675,
449 doi:10.1084/jem.20151948 (2016).
450 28 Sun, Y., Ip, P. & Chakrabartty, A. Simple Elimination of Background Fluorescence in
451 Formalin-Fixed Human Brain Tissue for Immunofluorescence Microscopy. *J Vis Exp*,
452 doi:10.3791/56188 (2017).
453

454

455

bioRxiv preprint doi: https://doi.org/10.1101/2023.02.28.530224; this version posted March 1, 2023. The copyright holder for this preprint (which was not certified by peer review) is the author/funder, who has granted bioRxiv a license to display the preprint in perpetuity. It is made available under aCC-BY 4.0 International license.

Figure Legends

Figure 1. Cortical microglia accumulate lipofuscin-like autofluorescence (lipo-AF) throughout life. a Method for assessing lipo-AF across laser lines in unstained tissue. **b** Representative images of lipo-AF signal in unstained tissue in the young adult P90 cortex. Scale bar = 5 μm. **c** Quantification of lipo-AF signal intensity across laser lines. Data presented as mean ± SEM, n = 3 mice. One-way ANOVA with Tukey multiple comparisons test (F = 9.711, df = 11); *p<0.05 **p<0.01. **d** Method for assessing lipo-AF within microglia. **e** Representative images of anti-IBA1 immunolabelled microglia (green) and lipo-AF (white) in the developing (P5, P15), young adult (P30, P60, P90), and aged (24 months) somatosensory cortex and neighboring visual and auditory cortices. The AF was excited by the 561 nm laser line. Scale bars = 5 μm. **f** Quantification of the percentage of cortical microglial with [0-0.1]% (dark blue), [>0.1-1.0]% (light blue), [>1.0-2.0]% (pink), or >2.0% (dark red) of their total volume occupied by lipo-AF. **f** Data represented as a mean, n = 4 mice P5–P90, n = 3 mice 24m. ***g-j*** The same data as **f**, but each bin is graphed separately. Data are presented as a mean ± SEM. One-way ANOVA with Tukey multiple comparisons test (**g**, F = 15.49, df = 22; **h**, F = 15.53, df = 22; **i**, F = 1.584, df = 22; **j**, F = 129.9, df = 22); *p<0.05 ***p<0.001 ****p<0.0001. **k** Quantification of the percentage of lipo-AF volume that is outside of microglia. Data represented as mean ± SEM, n = 4 mice P5–P90, n = 3 mice 24m. One-way ANOVA with Tukey multiple comparisons test (F = 24.51, df = 22); *p<0.05 **p<0.01 ***p<0.001 ****p<0.0001.

Figure 2. Microglial accumulation of lipo-AF signal is not exacerbated in a mouse model of neurodegeneration. a Methods for assessing lipo-AF in microglia in the 5XFAD mouse model. **b** Representative images of anti-IBA1 immunolabelled microglia (green), Thioflavin S labeled amyloid plaques (ThioS, magenta), and lipo-AF (white) in the somatosensory cortex of 9-month-old 5XFAD mice and wild-type (WT) littermates. The lipo-AF was excited by a 561 nm laser. Scale bars = 5 μm. **c** Quantification of the percentage of cortical microglial with [0-0.1]% (dark blue), [>0.1-1.0]% (light blue), [>1.0-2.0]% (pink), or >2.0% (dark red) of their total volume occupied by AF. Data are represented as the mean, n = 3 mice. **d-g** Same data as **c**, but each bin is graphed separately. Data are represented as mean ± SEM. One-way ANOVA with Tukey multiple comparisons test (**d**, F = 9.74, df = 8; **e**, F = 2.095, df = 8; **f**, F = 4.813, df = 8; **g**, F =0.04357, df = 8); *p<0.05.

bioRxiv preprint doi: https://doi.org/10.1101/2023.02.28.530224; this version posted March 1, 2023. The copyright holder for this preprint (which was not certified by peer review) is the author/funder, who has granted bioRxiv a license to display the preprint in perpetuity. It is made available under aCC-BY 4.0 International license.

29 **Figure 3. Methods to eliminate lipo-AF signal from mouse brain tissue. a** Methods for the post-
30 immunostaining quenching protocol using the commercially available TrueBlack Plus™ (TBP) reagent.
31 **b** Representative images of anti-P2RY12 immunolabelled microglia (green) and lipo-AF (white) in
32 untreated or TBP-treated samples from P90 mouse cortex. Scale bars = 5 µm. **c** Quantification of the
33 percentage of cortical microglial with [0-0.1]% (dark blue), [>0.1-1.0]% (light blue), [>1.0-2.0]% (pink),
34 or >2.0% (dark red) of their total volume occupied by AF. Data are represented as the mean. **d-f** Same
35 data as **c**, but each bin is graphed separately. Data are represented as a mean ± SEM, n = 3 mice.
36 Two-tailed unpaired t-test (**d**, $t = 8.912$, $df = 4$; **e**, $t = 9.679$, $df = 4$; **f**, $t = 0.9982$, $df = 4$); ***p<0.001. **g**
37 Quantification of the intensity of the anti-P2RY12+ signal in untreated (dark gray bar) or TBP-treated
38 (light gray bar) samples. Data are represented as a mean ± SEM, n = 3 mice. Two-tailed unpaired t-
39 test ($t = 4.698$, $df = 4$); **p<0.01. **h** Schematic describing the pre-immunostaining photobleaching
40 protocol. **I** Representative images of anti-P2RY12 immunolabelled microglia (green) and lipo-AF (white)
41 in untreated or photobleached samples from P90 mouse cortex. Scale bars = 5 µm. **j** Quantification of
42 the percentage of cortical microglial with [0-0.1]% (dark blue), [>0.1-1.0]% (light blue), [>1.0-2.0]%
43 (pink), or >2.0% (dark red) of their total volume occupied by AF. Data are represented as a mean, n =
44 3 mice. **k-m** Same data as **j**, but each bin is graphed separately. Data represented as a mean ± SEM.
45 Two-tailed unpaired t-test (**k**, $t = 19.63$, $df = 6$; **l**, $t = 9.235$, $df = 6$; **m**, $t = 1.156$, $df = 6$); ****p<0.0001.
46 **n** Quantification of the intensity of the anti-P2RY12+ signal in untreated (dark gray bar) or
47 photobleached (light gray bar) samples. Data presented as mean ± SEM, n = 4 mice. Two-tailed
48 unpaired t-test ($t = 1.886$, $df = 6$).

49 **Figure 4. Use of the photobleaching method to determine the degree to which lipo-AF signal can**
50 **confound analysis of engulfed synaptic material within microglia. a** P90 mouse brain sections
51 were immunolabeled with anti-VGluT2 antibody and secondary antibodies conjugated with Alexa-Fluor
52 594. Microglia were also co-immunolabeled with anti-IBA1. Adjacent sections were left unstained to
53 image AF. **b** Representative images of anti-VGluT2+ presynaptic terminals within the P90
54 somatosensory cortex immunolabelled with Alexa-Fluor 594 secondary antibody. The dashed orange
55 circles highlight the anti-VGluT2 signal outside microglia. The dashed yellow circles highlight the anti-
56 VGluT2 signal inside microglia. Bottom image is the same image without the anti-IBA1 immunostaining.
57 Scale bars = 5 µm. **c** Quantification of the fluorescence intensity of Alexa-Fluor 594 immunolabelled
58 VGluT2+ puncta, outside (orange bar) and inside microglia (yellow bar) upon excitation with a 561 nm

bioRxiv preprint doi: https://doi.org/10.1101/2023.02.28.530224; this version posted March 1, 2023. The copyright holder for this preprint (which was not certified by peer review) is the author/funder, who has granted bioRxiv a license to display the preprint in perpetuity. It is made available under aCC-BY 4.0 International license.

59 laser line. For comparison, lipo-AF signal intensity (gray bar), upon excitation with a 561 nm laser line,
60 in adjacent tissue sections was also quantified. Data are represented as a mean ± SEM, n = 3 mice.
61 One-way ANOVA with Tukey multiple comparisons test (F = 5.873, df = 8); *p<0.05. **d-e** Representative
62 images of signal in the anti-VGluT2+ immunolabeled channel (red) inside anti-CD68+ lysosomes (cyan)
63 of anti-IBA1 immunolabelled microglia (green) in untreated (left) or photobleached samples (right) from
64 P5 (d) or P90 (e) mouse cortex. White dotted circles highlight signal within the anti-VGluT2 channel that
65 co-localize with microglial C68+ lysosomes. Bottom images in d and e are the same images as the top
66 images without the anti-IBA1 immunostaining. Scale bars = 5 μm. **f** The ratio of the volume of apparent
67 engulfed anti-VGluT2+ material within microglia from the P5 and P90 mouse cortex post-
68 photobleaching to pre-photobleaching (volume of anti-VGluT2 signal within microglia post-
69 photobleaching/pre-photobleaching signal). Data are represented as a mean ± SEM, n = 4 mice. Two-
70 tailed Mann-Whitney t-test; *p<0.05.

71 **Fig. 5 Photobleaching quenches lipo-AF signal in mouse, marmoset and human brain tissue. a-**
72 **d** Representative images of lipo-AF upon excitation with a 488 nm, 561 nm or 638 nm laser line in
73 untreated (left column) or photobleached (right column) samples from 24-month-old mouse cortex (a),
74 9-month-old 5XFAD mouse cortex (b), 11-13 year-old marmoset cortex (c), and 60-77 year-old human
75 cortex (d). Scale bars = 5 μm. **e-h** Quantification of lipo-AF signal intensity before and after
76 photobleaching for each species. Data represented as a mean ± SEM, n = 3 biological replicates per
77 species. Two-way ANOVA with Šídák's multiple comparisons test (**e**, F = 114.7, df = 1; **d**, F = 69.41, df
78 = 1; **f**, F = 59.30, df = 1; **h**, F = 171.3, df = 1;); **p<0.01, ***p<0.001****p<0.0001.

79

bioRxiv preprint doi: https://doi.org/10.1101/2023.02.28.530224; this version posted March 1, 2023. The copyright holder for this preprint (which was not certified by peer review) is the author/funder, who has granted bioRxiv a license to display the preprint in perpetuity. It is made available under aCC-BY 4.0 International license.

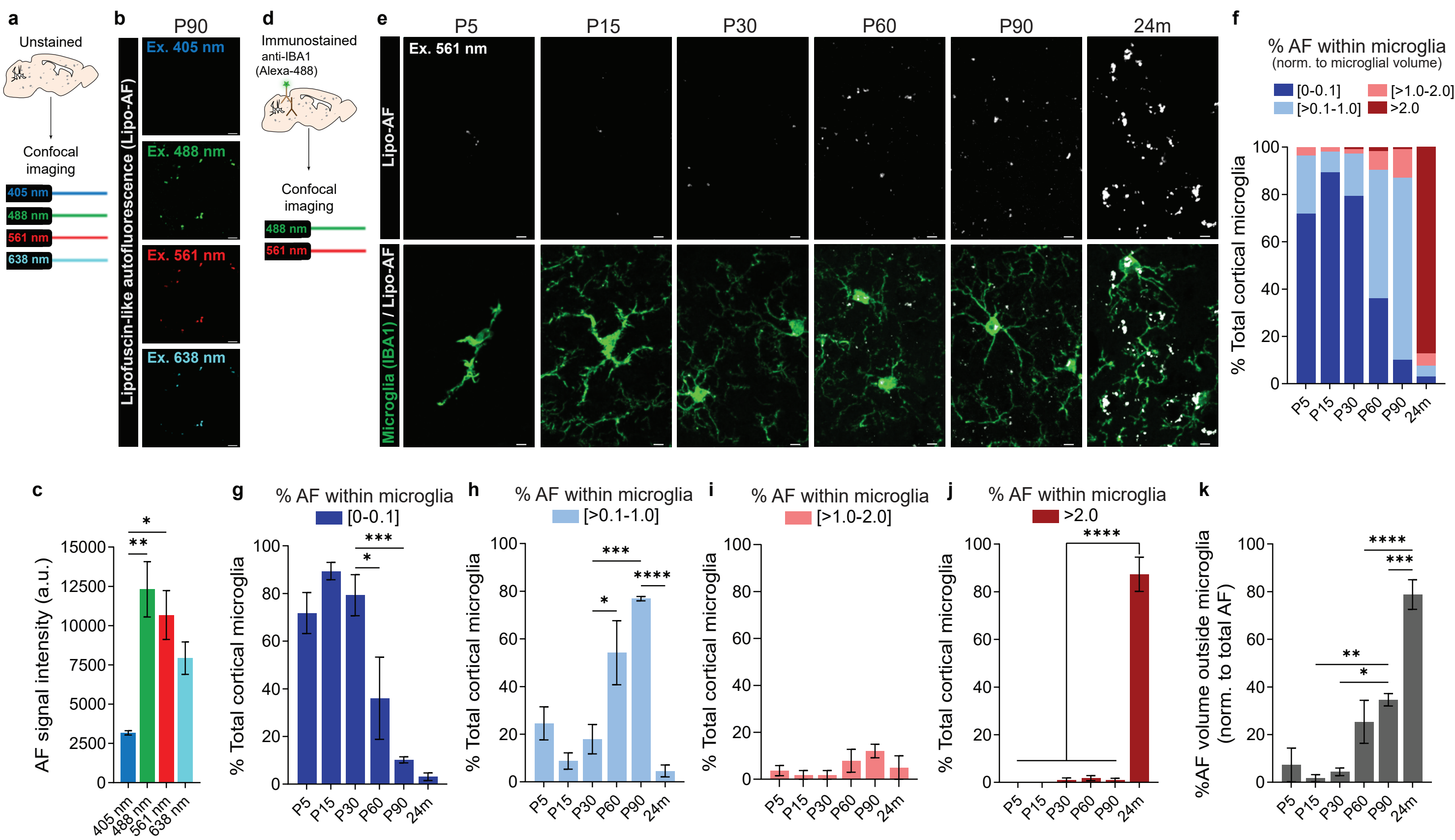

bioRxiv preprint doi: https://doi.org/10.1101/2023.02.28.530224; this version posted March 1, 2023. The copyright holder for this preprint (which was not certified by peer review) is the author/funder, who has granted bioRxiv a license to display the preprint in perpetuity. It is made available under aCC-BY 4.0 International license.

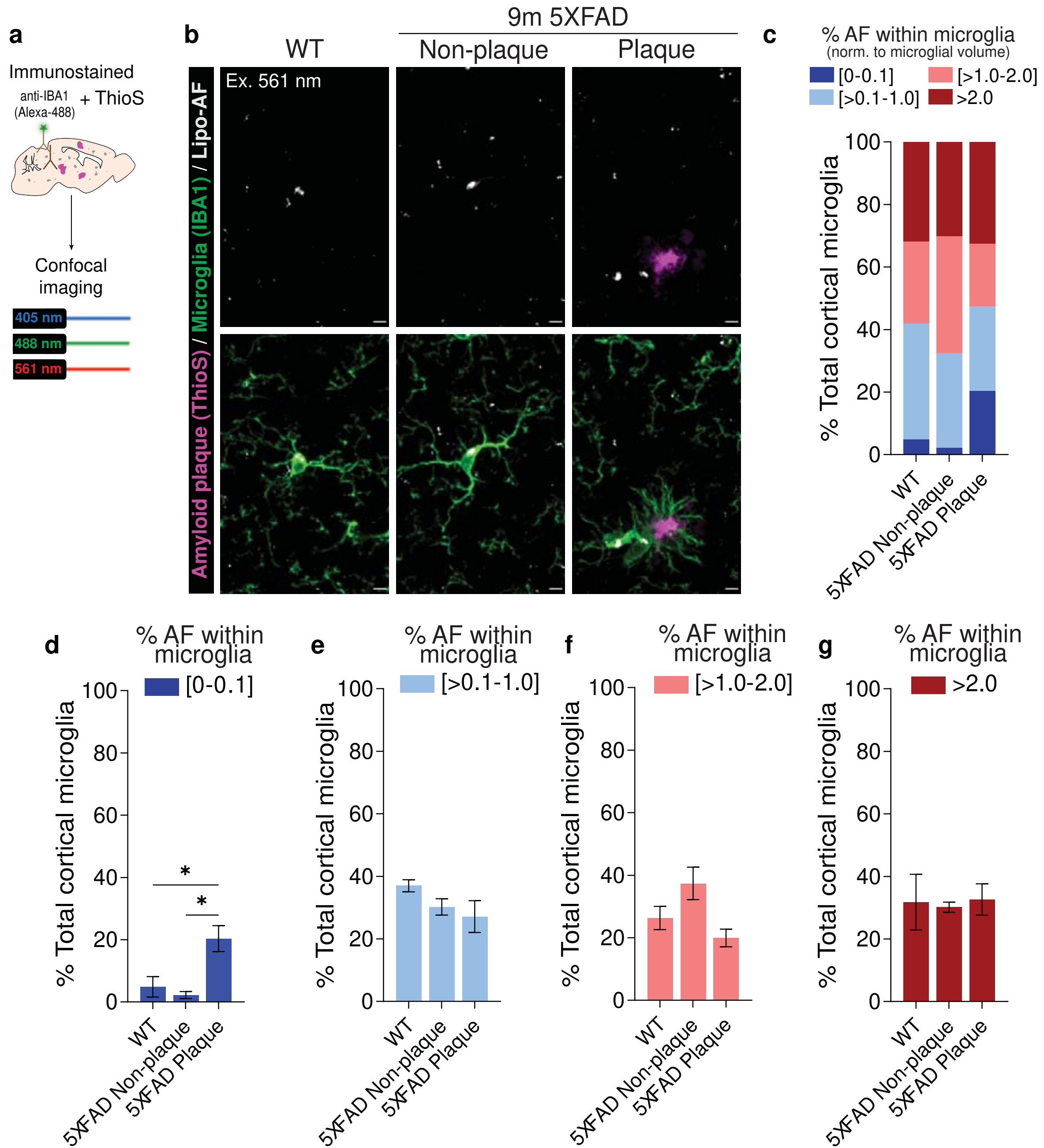

bioRxiv preprint doi: https://doi.org/10.1101/2023.02.28.530224; this version posted March 1, 2023. The copyright holder for this preprint (which was not certified by peer review) is the author/funder, who has granted bioRxiv a license to display the preprint in perpetuity. It is made available under aCC-BY 4.0 International license.

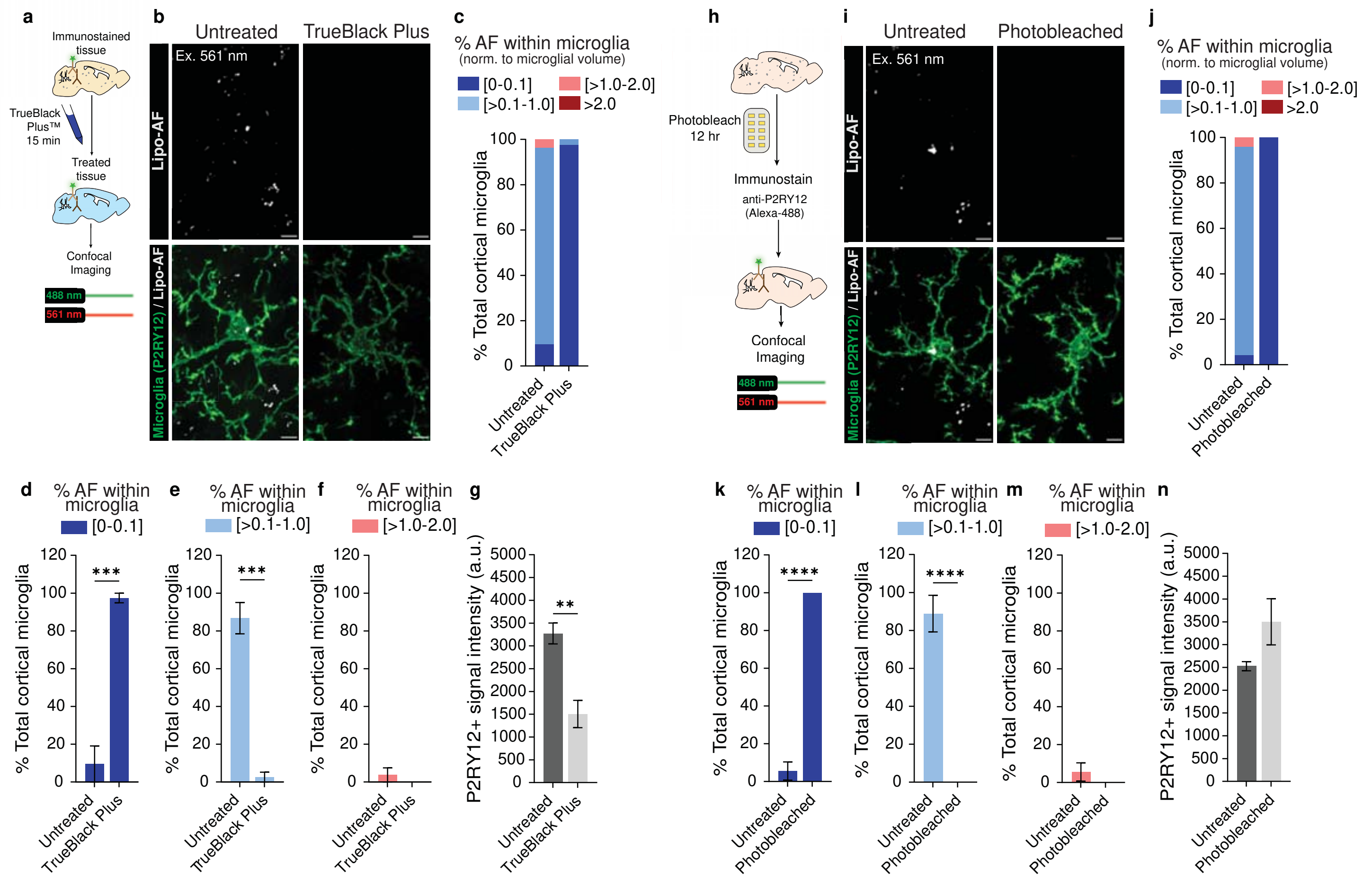

bioRxiv preprint doi: https://doi.org/10.1101/2023.02.28.530224; this version posted March 1, 2023. The copyright holder for this preprint (which was not certified by peer review) is the author/funder, who has granted bioRxiv a license to display the preprint in perpetuity. It is made available under aCC-BY 4.0 International license.

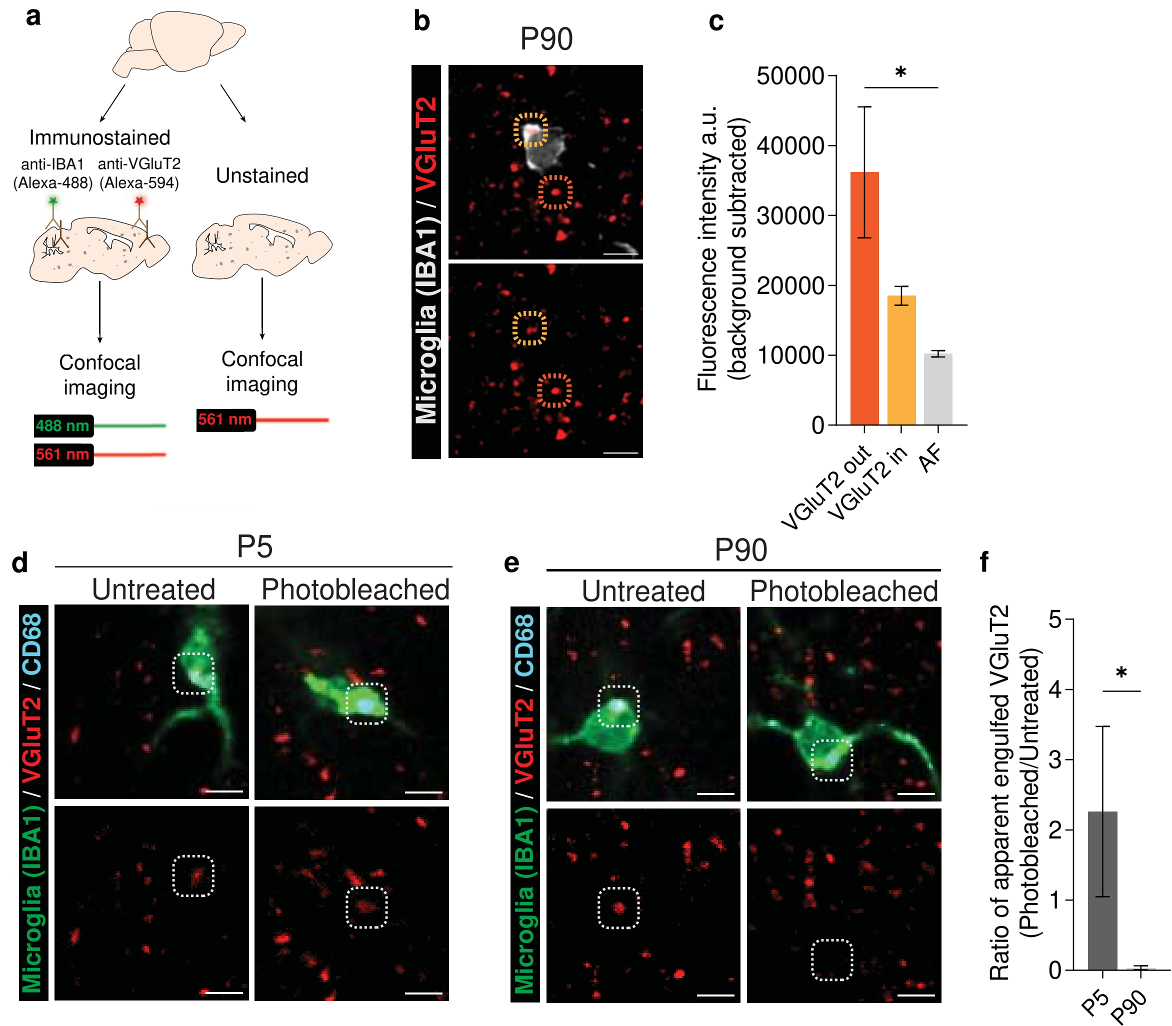

bioRxiv preprint doi: https://doi.org/10.1101/2023.02.28.530224; this version posted March 1, 2023. The copyright holder for this preprint (which was not certified by peer review) is the author/funder, who has granted bioRxiv a license to display the preprint in perpetuity. It is made available under aCC-BY 4.0 International license.